Accurate Joule Loss Estimation for Rotating Machines: An Engineering Approach

Adeeb Ahmed
Department of Electrical and Computer Engineering
North Carolina State University
Raleigh, NC, USA
aahmed4@ncsu.edu

Iqbal Husain
Department of Electrical and Computer Engineering
North Carolina State University
Raleigh, NC, USA
ihusain2@ncsu.edu

***Abstract*— Detailed analysis of thermal aspects of rotating machine joule loss production is presented. A step-by-step guideline is proposed to precisely separate the electric loss components in rotating machines. The procedure is illustrated for a permanent magnet motor with transverse flux topology but the methodology is equally applicable for conventional radial flux machines with or without magnets. Identifying the responsible factors for loss generation can be useful for further improvement of the topology before going for final production. The method has been applied to the prototype motor; motor efficiency, loss map, and separated loss components are provided as a function of torque and speed.**

Keywords—Permanent magnet machines, AC machines, motor drives, loss separation, joule loss, loss components

I. Introduction

Permanent magnet motors are gaining popularity with the growing need of more efficient and high-performance applications. In recent years, permanent magnet synchronous machines with variable speed drives are replacing the old school line-start induction machines both for better overall performance and the decreasing cost of voltage source inverters. With some inherent advantages, permanent magnet machines also pose challenges when a reliable loss model is required. Though FEA based loss model using Steinmetz's equations are often used, the practical machine losses often exhibit significant deviations that make the performance estimation extremely difficult [1]. Even with the prototype available, accurately separating the losses for a better understanding of the responsible contributors can be a difficult task considering the non-idealities and practical constraints. Most importantly, with the change in the operating temperature, the motor parameters change significantly creating additional difficulties in the measurement and separation method. Although it appears as a straightforward approach, separation of copper loss contribution from total loss can be challenging due to the change in winding resistance and the difficulty in measuring the change with temperature variation.

Different approaches have been previously undertaken to separate the loss components in permanent magnet machines [2,3,4,5]. In some of these cases, finite element analysis (FEA) based approach was adopted [1,5]. A calorimetric measurement based approach was proposed in [4] which enables identifying the core loss at different frequencies. In [5], separation of eddy current loss was demonstrated but the process requires a separate rotor with removed magnets which poses additional challenges in setting up the experimental platform. A combination of FEA and experimental method and more elaborate loss separation method has been proposed in [2] which attempted separation of loss components depending on their order of relationship with excitation current and operating frequencies. Regardless of the methods applied, the isolation of the joule loss component from the total loss is a prerequisite and the accuracy in this procedure is essential. In this work, a simple and straightforward approach will be demonstrated to precisely separate the joule loss component from the total loss. The procedure requires no additional hardware setup and can be easily automated. Application of the procedure provides an efficient approach to accurately model the joule loss component which can be further used in all other test procedures.

II. Thermal Contribution in Loss Component

Among the different factors of operating conditions, variation in temperature is the dominant contributor in adding complexity to loss measurement. Change in temperatures can affect the losses in different ways, and the following factors can be considered the most significant:

i) Copper loss variations due to change in winding resistance
ii) Magnetic loss variations due to change in magnet properties such as change in remnant flux density
iii) Lamination material properties (such as conductivity causing eddy current loss) that further changes the magnetic loss components.

Although seems simple, isolating the copper loss component from the total loss can be difficult due to temperature variation during the experiment. Moreover, local hotspots and non-uniform winding temperature complicate the process of temperature measurement and resistance estimation. In some literature, methods have been proposed to estimate the winding resistance for induction machine based on motor models [6,7], but these methods do not guarantee an accurate estimation. Signal injection based methods can be another option, but this requires injecting a DC current in the system that can result in torque ripple. In addition, the DC injection requires a neutral connection in the system adding complexity to the system [6,8]. Methods have been suggested in IEEE Std. 112 [9], developed for poly-phase induction machines, to measure accurate temperature, and methods have been prescribed for permanent magnet motors in IEEE Std. 1812-2014 [10] as well. The standards provide means to effectively measure line-to-line resistance after the shutdown of the motor at a certain temperature and thus create an approximate mapping of the line-to-line resistance with the embedded

978-1-4799-7312-5/18/$31.00 ©2018 IEEE

temperature measurement. But the procedure does not account for variation of phase-to-phase resistance due to non-uniform winding cooling and thus an improvement in the procedure is conceivable. In this paper, a straightforward approach will be provided to get a more accurate representation of winding resistance as a function of embedded detector temperature readings.

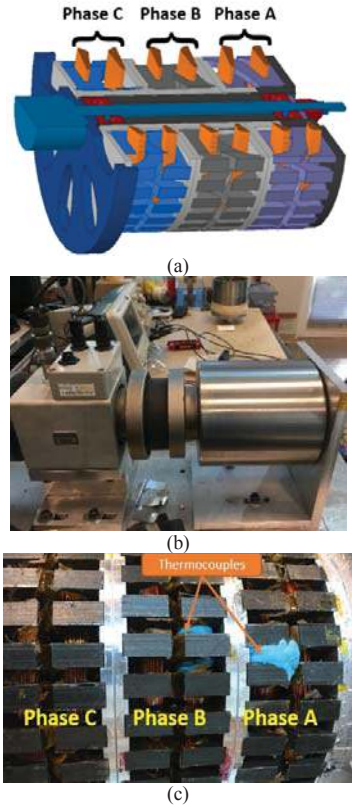

Fig. 1. Experimental outer rotor PM Transverse Flux Motor (a) Schematic of the cross-section with the rotor removed (b) Full prototype motor in test bench (c) Prototype motor stator and thermocouple placements for phase A, phase B and phase C (opposite side).

III. Temperature Contribution in Joule Loss

In most cases, joule loss or copper loss is the simplest form of loss to be measured given that the excitation frequency is low enough not to produce any AC copper loss. In cases where all coils are uniformly placed and experience similar natural or forced cooling, winding resistances of all phases can be considered nearly identical. Thus, a uniform sinusoidal excitation will result in a DC waveform for copper loss component. In such cases, a line-to-line resistance measurement according to IEEE Std. 112 is sufficient for winding resistance estimation at certain temperatures. However, the uniform winding cooling might not be the case for all motor structures and the unpredictability of heat extraction both for forced and natural cooling can add complexity to the system. An outer rotor motor structure with transverse flux topology is presented in Fig. 1. Fig. 1(a) shows the illustration of the cross-section of the motor with removed rotor. The three-phase motor contains six ring-shaped coils and a pair of coil forms one phase winding. As seen in Fig. 1(b), the motor is mounted with Phase A winding being the closest to the mounting plate and vice versa. Since air acts as a thermal insulator, the air gap of the motor passes a small amount of heat making the mounting plate the true heat-sink in the system. This causes a large temperature gradient in the system resulting in a significant difference between the phase resistances. Details about this motor topology can be found in [11,12] and this literature focuses on the experimental procedures developed to address issues that arose during the prototype performance testing. The problem can be realized in radial flux machines as well with conventional windings especially for forced cooling system depending on the motor mounting orientation and placement of cooling nozzles. Experimentally measured copper loss for the prototype is shown in Figure 2(a). It should be noted that the eddy current loss in the copper was ignored in the process which is acceptable for the majority of cases. The motor was excited with a perfectly sinusoidal current of 0.015 Hz to eliminate any magnetic loss component. The corresponding copper loss exhibits a second order oscillation and the peak copper loss coincide closely with the peak value of the phase C current. This indicates a significant increase in phase C resistance compared to other phases. Since there are only three unknowns, a time-varying acquisition of the loss data can be used to form the linear equations to estimate phase resistance values. Thus, assuming constant resistivity for three consecutive time steps, the phase resistances' relationship with losses can be expressed as

$$[R_a(t)\ R_b(t)\ R_c(t)]^T = A(t)^{-1} P_{cu}(t) \quad (1)$$

where $A(t) = \begin{bmatrix} I_a^2(t-T_S) & I_b^2(t-T_S) & I_c^2(t-T_S) \\ I_a^2(t) & I_b^2(t) & I_c^2(t) \\ I_a^2(t+T_S) & I_b^2(t+T_S) & I_c^2(t+T_S) \end{bmatrix}$

and $P_{cu}(t) = [P_{cu}(t-T_S) \quad P_{cu}(t) \quad P_{cu}(t+T_S)]^T$

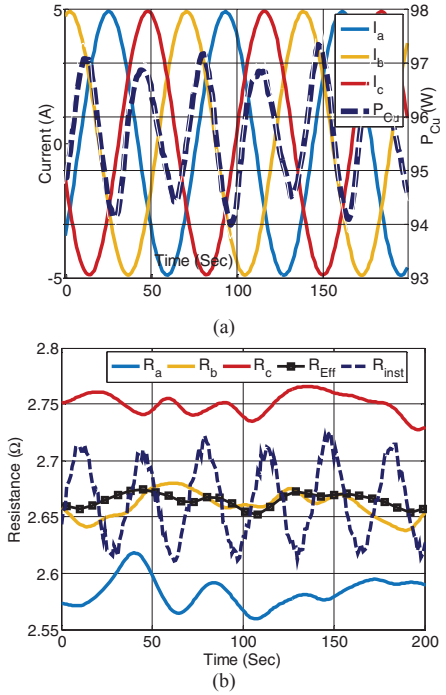

Fig. 2. (a) Three phase sinusoidal excitation of 0.015 Hz. The dotted line represents the copper loss variation (b) Three phase resistance found using Eqn. 1.

Figure 2(b) shows the computed resistance for the 200 sec. time interval using Eq. 1. The significant variation in phase resistance is obvious from the plot where phase-C resistance is found to be more than 7% higher than that of phase-A. R_{inst} in Fig. 2(b) represents the instantaneous effective resistivity considering the current vector and can be expressed as

$$R_{inst(t)} = \frac{P_{Cu}(t)}{I_a^2(t) + I_b^2(t) + I_c^2(t)} \quad (2)$$

For a reasonable speed operation, this instantaneous resistivity value is not required, and the cycle average value is sufficient which can be readily available by averaging the three phase resistances and denoted as R_{Eff} in Fig. 2(b). R_{Eff} eliminates the current dependence on the resistivity and is the true effective resistance for balanced excitation. The scope of this paper concentrates in a simple and effective way to represent this R_{Eff} as a function of measured temperatures at different locations.

IV. Experimental Setup and Test Procedure

The proposed procedure requires a simple setup with no modification in the motor. The motor shown in Fig. 1 is simply connected with the inverter driver with no load connected to the shaft. Basic motor parameters of the experimental motor are provided in Table I. Instead of using position feedback, the motor is excited with a constant frequency sinusoidal excitation with extremely low frequency. In the actual experiment, a sinusoidal excitation of 0.015 Hz was used, which resulted in a slow rotor movement with constant angular speed (0.056 RPM). This enables to assume zero mechanical output power as the rotor is always aligned with the *d*-axis yielding no mechanical torque output. Four thermocouples were placed to measure the temperatures at different locations. The temperature readings for the thermocouples placed at phases A, B, C, and the mounting plate are shown in Fig. 3(a). It should be noted that for phase-A, the thermocouple was placed between the coil and the stator pole making this reading slightly smaller than actual coil temperature. Even for other phases, depending on the contact region of the thermocouples, motor mounting orientation and other mechanical factors, the sensor temperature readings are not necessarily the effective coil temperature. To come up with the actual effective coil temperature T_{Eff}, a weighted average of the temperature readings was taken to calculate the effective temperature T_{Eff}. Technically, T_{Eff} can be referred as the weighted average of all the temperature readings and represents the effective coil temperature, given that the phase resistances can be represented by a single equivalent resistance.

$$T_{Eff} = \sum \sigma_n T_n \quad (3)$$

$$R_{Estimate} = R_{EstimateREF}[1 + (T_{EffREF} - T_{Eff})\alpha_{Cu}] \quad (4)$$

$$J = \frac{1}{N}\sum_n \left(R_{Estimate} - R_{Eff}\right)^2 \quad (5)$$

where $R_{EstimateREF}$ is the effective resistance R_{Eff} computed using Eqn. 1 (average of three phase resistances) at any reference point and T_{EffREF} is the effective coil temperature using Eq. 3 at the same reference point. T_n's are the temperature sensor readings for different thermocouples and α_{Cu} is the copper resistivity temperature coefficient. Values for the weight coefficients σ_n are obtained to minimize the objective function J which is the mean squared error (MSE) between the computed R_{Eff} and the estimated value $R_{Estimate}$. Once the weight coefficients are evaluated for the motor with certain sets of embedded sensors, the same coefficients can be used throughout the experiment to precisely isolate joule losses from the total loss. This ensures a full mapping of effective resistance values with thermocouple readings for the whole thermal operating range of the motor.

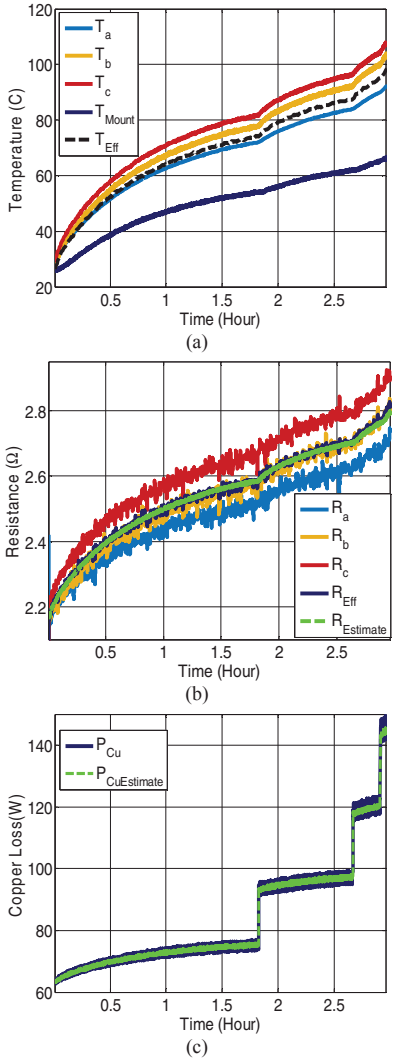

Fig. 3. (a) Thermocouple temperature reading for resistance mapping test procedure (b) Calculated phase resistances for three phases and the weight function estimated value $R_{Estimate}$ (c) Measured and estimated copper loss throughout the process.

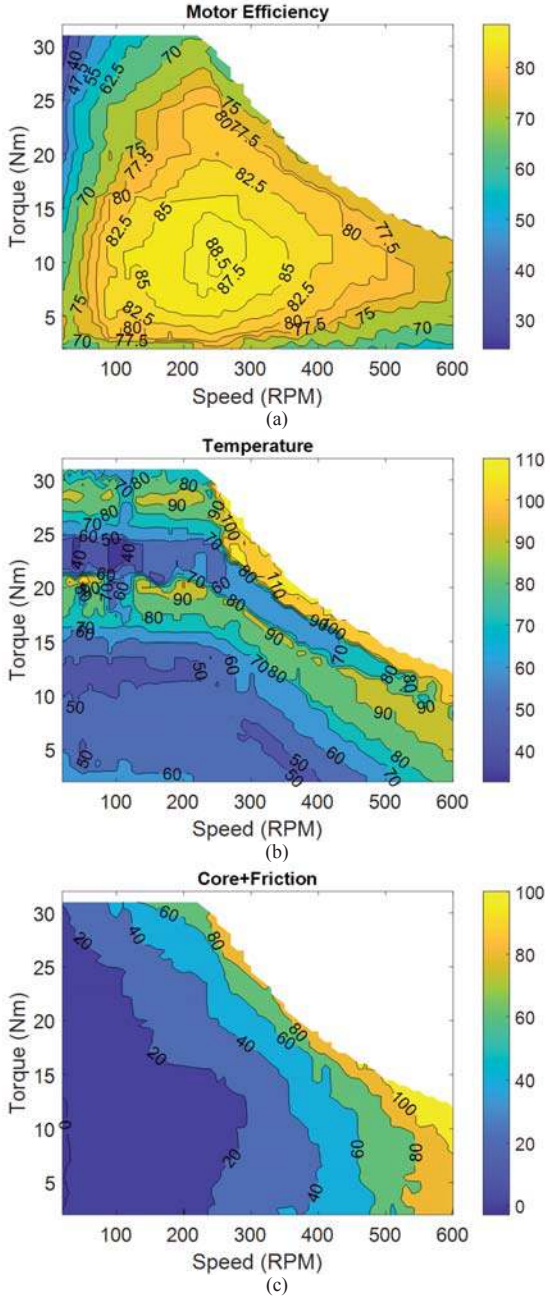

Fig. 4. (a) Motor efficiency map using maximum torque per ampere control (b) Measured effective temperature while generating the efficiency plot (c) Magnetic and other losses after joule loss separation.

The plots collected during the resistance mapping test procedure are shown in Fig. 3(a) through (c). Temperature readings during the test procedure are shown in Fig. 3(a). Since the input power consists of only joule loss at this frequency, the effective phase resistance values were computed using Eq. (1) and shown in Fig. 3(b). This provided the desired R_{Eff} also shown in Fig. 3(b) and by minimizing the objective function, appropriate weight functions were computed to come up with $R_{Estimate}$ as a function of T_n s. The estimated copper loss using this estimated resistance is shown in green in Fig. 3(c) and denoted as $P_{CuEstimate}$. It should be noted that the measured copper loss P_{Cu} has the second order sinusoidal variation (as shown in Fig. 2(a)) captured in the measurement due to extremely low frequency current and relatively faster sample rate for power measurement. But the mean value of the copper loss has precise correspondence with the estimated value. The step nature of the measured and estimated copper loss is due to the step increase in current magnitude. Unless the temperature sensors are not physically moved to different locations, the weight function computed in the procedure can be used for future motor testing.

TABLE I. MOTOR PARAMETERS AND PERFORMANCE

Peak torque (Nm)	32
Corner speed (RPM)	240
DC bus voltage (V)	250
Peak RMS current (A)	5.67
Power factor (@ corner speed, peak torque)	0.7
Magnet type	N42
Number of poles	32

A typical application of the proposed joule loss estimation method is the determination of an electric machine performance, effective temperature rise and other loss estimation over the entire torque-speed operating range as presented in Fig. 4 (a), (b), and (c). The efficiency plot of the motor over the torque-speed range operated with vector control method is presented in Fig. 4(a). Due to variation in operating conditions throughout the experiment, the temperature of the system kept changing and the corresponding temperature for each torque speed points are also stored simultaneously and plotted in Fig. 4(b). It should be noted that the corresponding temperatures for each torque-speed node are not necessarily the steady state temperature at those points. But as the temperature data is available, the coefficient tuned in the previous low-frequency excitation test can be used to precisely compute the effective winding resistance, and therefore, the copper loss. The summation of magnetic and friction windage loss at different operating points are shown in Fig. 4(c). This map can be computed simply by subtracting the estimated joule loss from the total measured loss. In an ideal scenario, the summation of friction and magnetic loss should converge to zero at zero speed given that the joule loss is accurately measured. However, in Fig. 4(c), a small region can be found with negative magnetic loss which represents slight overestimation of the joule loss component. The magnitude of this error is relatively small and occurs in a minute region and thus demonstrates the accuracy of the method. Underestimation of joule loss would have created a region with a positive non-zero magnetic loss at zero speed. Measurement of mechanical power at this low speed also poses challenges and can contribute to error in

measurement. In most cases, calculating the loss components in a single operating point cannot provide any mean to measure the accuracy of joule loss estimation. Inaccuracy in joule loss estimation is often not identified and consequently, creates an incorrect estimation of magnetic loss components.

V. Conclusion

A straightforward approach is presented to accurately model the phase resistance as a function of embedded sensor readings. The procedure requires no additional hardware setup rather than typical test setup used in efficiency measurement. The temperature weight function in the resistance estimation process ensures accuracy even with poor thermocouple placement. The added accuracy in the joule loss isolation is the first step towards the isolation of other magnetic loss components.

References

[1] T. Sakaue, and K. Akatsu, "Stator iron loss measurement method in permanent magnet synchronous motor to remove the mechanical loss effect." *Electrical Machines and Systems (ICEMS), 2014 17th International Conference on*. IEEE, 2014.

[2] G. Heins, et al. "Combined Experimental and Numerical Method for Loss Separation in Permanent-Magnet Brushless Machines," *IEEE Transactions on Industry Applications* 52.2 (2016): 1405-1412.

[3] P. Sergeant, et al. "A computationally efficient method to determine iron and magnet losses in VSI-PWM fed axial flux permanent magnet synchronous machines." *IEEE Transactions on Magnetics,* 50.8 (2014): 1-10.

[4] D. Singh, and A. Arkkio. "Calorimetric measurement of stator core losses." *Electrical Machines (ICEM), 2012 XXth International Conference on*. IEEE, 2012.

[5] K. Yamazaki, et al. "Investigation of locked rotor test for estimation of magnet PWM carrier eddy current loss in synchronous machines." *IEEE Transactions on Magnetics,* 48.11 (2012): 3327-3330.

[6] S. B. Lee, et al. "An evaluation of model-based stator resistance estimation for induction motor stator winding temperature monitoring." *IEEE Transactions on Energy Conversion* 17.1 (2002): 7-15.

[7] C.B. Jacobina, J. E. C. Filho, and A. M. N. Lima, "On-line estimation of the stator resistance of induction machines based on zero sequence model," *IEEE Trans. Power Electron*ics, vol. 15, pp. 346–353, Mar. 2000

[8] D.A. Paice "Motor thermal protection by continuous monitoring of winding resistance." *IEEE Transactions on Industrial Electronics and Control Instrumentation* 3 (1980): 137-141.

[9] IEEE Std 112-2004 - IEEE Standard Test Procedure for Polyphase Induction Motors and Generators

[10] IEEE Std 1812-2014 - IEEE Trial-Use Guide for Testing Permanent Magnet Machines

[11] A. Ahmed, Z. Wan, I. Husain, "Permanent Magnet Transverse Flux Machine with Overlapping Stator Poles", IEEE Energy Conv. Cong. and Expo. ECCE, 2015.

[12] A.Ahmed, I. Husain. "Power factor improvement of a transverse flux machine with high torque density," *IEEE Transactions on Industry Applications* (2018).